Supplementary materials for

Rapid degradation behavior of the encapsulated perovskite solar cells under the light, bias voltage or heat fields

Xiaobo Zhang[1], Xiaoqing Chen*[2], Yichuan Chen[1], Nabonswende Aida Nadege Ouedraogo[1], Jingjie Li[1], Xiulong Bao[3], Chang Bao Han[1], Yasuhiro Shirai[4], Yongzhe Zhang*[2], Hui Yan[1]

[1]Faculty of Materials and Manufacturing, Beijing University of Technology, Beijing 100124, China.

[2]Key Laboratory of Optoelectronics Technology, Ministry of Education, Faculty of Information Technology, Beijing University of Technology, Beijing 100124, China

[3]School of Electrical and Electronic Engineering, Beijing-Dublin International College (BDIC), University College Dublin, Ireland

[4]National Institute for Materials Science (NIMS), 1-1 Namiki, Tsukuba, Ibaraki, 305-0044, Japan

*Corresponding authors. E-mail addresses: chenxiaoqing@bjut.edu.cn (Xiaoqing Chen), yzzhang@bjut.edu.cn (Yongzhe Zhang),

1.Experiment

1 .1 Materials

The tin oxide (SnO_2, 15% in H_2O) colloid precursor was purchased from Alfa Aesar. Related solution such as dimethyl sulfoxide (DMSO), N, N-dimethylformamide (DMF), isopropanol (IPA), acetonitrile, 4-tertbutylpyridine (4-TBP), and chlorobenzene (CB) were obtained from Sigma-Aldrich. The involved organic salts include methylammonium iodide (MAI, >99.5%), formamidinium iodide (FAI, >99.5%), formamidinium bromide (FABr, >99.5%), and, methylammonium chloride (MACl, >99.5%), aladdin phenylethylammonium iodide (PEAI, >99.5%), together with the spiro-OMeTAD (>99.5%) and lead iodine (PbI_2， >99.99%), which

were also purchased form Xi'an Polymer Light Technology Corp. Polymethylmethacrylate (PMMA) was ordered from Aladdin. All reagents and solvents were used as received.

1.2 Device fabrication

ITO substrates were cleaned by a sequential sonication treatment in the deionized water, acetone and isopropanol for 15 min, followed by ultraviolet-ozone treatment for 15 min. After that, 3.67% SnO_2 (diluted by water) solution was coated on the cleaned substrate at 2,000 rpm for 30 s, followed by annealing under 150 ℃ for 30 min in the air. 600 mg of PbI_2 was dissolved in 950 μL DMF and 50 μL DMSO. Organic salts (FAI:MAI:FABr:MACl = 56 mg:34 mg :10 mg :10 mg) were dissolved in 1 mL IPA. The perovskite layers were then fabricated by using a two-step spin-coating process reported previously (first step 1500 r.p.m. for 30 s; second step 2000 r.p.m for 30 s). Then the substrates were annealed at 70 ℃ for 1 min in the glove box (first step) and under 150 ℃ for 15 min in the air environment (humidity = 30~40%). After that PMMA (5 mg/L) and PEAI (5 mg/L) IPA solution were spin coated on the perovskite layers (5000 r.p.m for 30 s) and then annealed under 70 ℃ for 5 min. The hole transport layers (HTL) were deposited by spin coating the spiro-OMeTAD solution (90 mg spiro-OMeTAD in 1 mL CB and mixing 10 μL 4-TBP and 35 μL LiTFSI (260 mg/mL in acetonitrile)). The above solutions were spin coated on the perovskite layers (3,000 r.p.m for 30 s). Finally, 80 nm Au electrode was evaporated under a high vacuum of $8*10^{-4}$ Pa. Our PSCs of area is 0.1 cm^2 and aperture area of 0.04 cm^2.

1.3 Characterization of Device and Materials

The current density–voltage (*J-V*) measurement was performed via a Keithley 2400 Source Meter under a solar simulator (AM1.5G). The external quantum efficiency curves were obtained with a Zolix SCS10-X150-DSSC system. Electrochemical impedance spectroscopy (EIS) results were obtained by electrochemical workstation under different external field conditions (bias voltage, light intensity, heated temperature). In these EIS measurements, the device impedance was measured by applying 10 mV AC voltage of which the frequency was swept from 1 Hz to 1 MHz. EIS results are presented as a Nyquist plot, with the real imaginary part (Z') as the abscissa and the negative imaginary part (Z'') as the ordinate. In addition, the -Im(Z) and frequency relationships were also shown to highlight the resonance time values. Capacitance–voltage relationships were measured under 10 mV AC voltage at 1 kHz. The surface morphology was obtained using a field-emission scanning electron microscopy (SEM, Hitachi, SU8010), using an electron beam accelerated at 5 kV. The X-ray diffraction (XRD) patterns were recorded using Cu-K_α conventional

pattern (XRD, Bruker D8 Advance, λ=1.5406 Å). The absorption spectra were recorded with Jasco V-670.

1.4 Analysis of the validation and prerequisites for using the M-S measurements

According to the Gauss' Law in the Maxwell equation

$$\rho = \frac{\varepsilon_0 \varepsilon_r dE}{dx} \quad (1)$$

and the definition of electric field

$$E = \frac{dU}{dx}, \quad (2)$$

the M-S relationship could be derived based on a few assumptions. Two most critical assumptions are 1) the device dopants are uniformly distributed and 2) the device thickness is wider than the depletion region. The latter assumption also requires that the doping density is larger than a value discussed in Ref. 1.[1] These two critical assumptions are sequentially discussed below.

1. The uniformity assumption. In the practical condition and our work, this assumption cannot be strictly ensured. In this regard, the calculated dopant density (N) can deviate from the real condition. However, the physical meaning of N is clear, which is the number of dissociated dopants in the depletion region. We would like to note that, we only analyzed the relative change of the effective statistical N, disregarding its spatial distribution. Therefore, such analysis should be reasonable.

2. The depletion region width assumption. According to the conclusion of the suggested reference, the M-S analysis was applicable under two conditions.

1) The doping density under research is away from the interface and inside the perovskite bulk. This condition is apparently satisfied in our condition because we use the M-S equation only to analyze the static bulk dopants.

2) The calculated density is larger than a minimum value described as[1]

$$N_{d,min} = \frac{27 m k_B T \varepsilon_r \varepsilon_0}{4 q^2 d^2} . \quad (3)$$

This condition is illustrated by the green shaded region of Figure S1. According to the thickness of our perovskite film (800 nm), this corresponding minimum charge densities value is about 5~8 × 10^{14} cm^{-3}. Considering our calculated N (10^{16} cm^{-3}), our condition on Figure S1 is the red circle which is well inside the green region. This means that our value is within the 'experimentally accessible region' suggested by Ref. 1. In addition, using the 10^{16} cm^{-3} doping concentration, the theoretical space-charge layer width at the onset of the linear M-S region would be $\omega \approx 500\,nm$—that is, smaller than the perovskite thin film's thickness, implying that our condition satisfies the required depletion width ($\omega \leq d$). Based on the above-mentioned analysis, we think that the doping density calculated by our C-V results can attribute to a response from doping or charged defects, instead of from geometrical capacitance or charge injection, implying that our M-S analysis agree with Ravishankar's opinion. In summary, rules are provided here to avoid to yield incorrect outcomes due to ignoring to prerequisites.

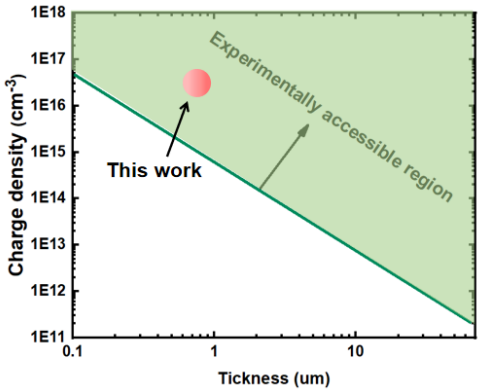

Figure S1. Minimum charge densities (dopant or trap) that will be observed in a capacitance-voltage measurement (m = 2 is assumed) for different thicknesses perovskite (olive) solar cells. The green region represents charge densities that are experimentally accessible for the perovskite solar cell. Fig. S1 of Ref. 1.

2.Supplementary experimental results

2.1 Analysis of solar cells performance

To evaluate the influence of these optimization on photovoltaic performance, we studied the electric property of PSCs based on reference and control devices at a scan rate of 50 mVs^{-1}. The *J-V* characteristics of champion devices are shown in Figure S3a while the performance parameters are summarized in Table 1. From Table.1, comparing the three devices, a slight drop in short-circuit current for modified cells can be found due to decrease in light absorption, confirmed by EQE curves as shown as Figure S4a and ultraviolet-visible spectrum (Figure S4b). The mismatch between the integral current obtained from EQE (24.22 $mAcm^{-2}$ of reference device, 23.66 $mAcm^{-2}$ of PEAI

device, 23.11 $mAcm^{-2}$ of PMMA device) and the short-circuit current of the *J-V* curve is less than 5%, indicating the feasibility of our IV curve results. Figure S3b shows the box line of the PCE extracted from reverse-scan *J-V* measurements. It is clear that the significant impact of the optimization is to increase the PCE. The average PCE of the reference 16.7%. This increases to 18.1% with PEAI device, and 18.8% for PMMA device, respectively corresponding to a relative increase of 8.4% and 12.6% compared to that of reference. The improved PCE can be mainly ascribed to elevated FF because of the reduced trap density. In order to confirm the suppression of electric traps by the passivation layer, we fabricated an electron-only device with the configuration of ITO/SnO_2/perovskite (with or without modified layer)/PCBM/Au. The double logarithmic *J-V* plots (Figure S4c, d and e) were measured under dark conditions. According to space-charge limited conduction (SCLC) theory[1], we can know the V_{TFL} values of perovskite films, PEAI and PMMA modified perovskite films were 0.67, 0.62 and 0.58 V, respectively. Based on our previous report[2], the corresponding electric trap densities were to be 3.57×10^{15}, 3.30×10^{15} and 3.09×10^{15} cm^{-3}. In addition, the relationship between V_{OC} and light intensity is (Figure S4f) analyzed to compare the ideality factor of the reference device (1.88) and the treated devices show a much smaller ideality factor (1.54 PEAI device, 1.63 PMMA device), where K_B is the Boltzmann constant and T is temperature.[2,3] The lowered ideality factors of the modified devices indicate suppressed trap-assisted recombination (SRH recombination) in the devices.[1] This result suggests our optimization layer (PEAI or PMMA) can suppress defect density, resulting in the improved FF. Meanwhile, as Figure S4g shown, hysteresis index of control cells is slight lower than that of reference cells, suggesting our modified layer can suppress the ion migration.[3]

2.2 mobile ions accumulation at the interface

Typically, both experiment and theory suggest that more than one type of ionic species are present in most commonly used perovskite materials. These different ionic species have distinctly different diffusion coefficients which may vary by orders of magnitude, and therefore could be categorized as 'slow' or 'fast' mobile ionic species. As addressed in the introduction paragraph, in this article, we mainly study the PCE degradation after more than 10^2 seconds of light, bias voltage and heat field processing. This timescale is apparently longer than the migration time of the halide ions across the perovskite layer (800 nm) which is typically 10^{-1} - 10^2 s.[4,5] However, it is comparable to the migration time of the organic cations (above 10^2 s). Therefore, we believe that the initial rapid PCE degradation process, of which the timescale is above 10^2 s mainly comes from the migration of the organic cations (MA^+/V_{MA} and FA^+/V_{FA}, next the MA^+/V_{MA} will be took as an example). The initial condition (S2a) describes a stoichiometric amount of anion and cation defects, which are randomly distributed in the perovskite lattice. (S2b) After the device was exposed to light or bias for up to 10^2 s (i.e. seconds ~ minutes), halide defects migrate and accumulate to the interface (perovskite/HTL and perovskite/ETL), leaving the relatively immobile cation defects behind. (S2c) After the device was exposed to light or bias for longer than 10^2 s (i.e. minutes ~ hours), cation defects accumulate at both interfaces (perovskite/HTL and perovskite/ETL). To conclude, when PSCs are exposed to light or bias (above 10^2 s), the slow cation defects migration is responsible for

the reversible losses in the device on the timescale of hours. At this point, the direction of the internal electric field is from ETL to HTL. Consequently, MA^+ ions accumulated at HTL/perovskite and V_{MA} ions at ETL/perovskite.

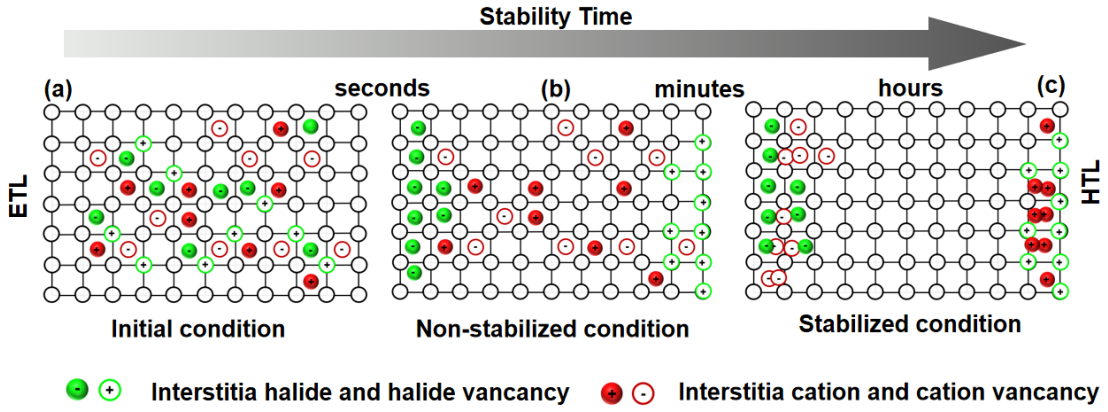

Figure S2. Schematics of the evolution of the ion distribution within the perovskite layer sandwiched between the electron (left) and hole transport (right) layer under solar cell similar working conditions (The direction of the electric field is from ETL to HTL): (a) initial condition, (b) non-stabilized condition on the timescale of minutes and (c) the stabilized condition on the timescale of hours.

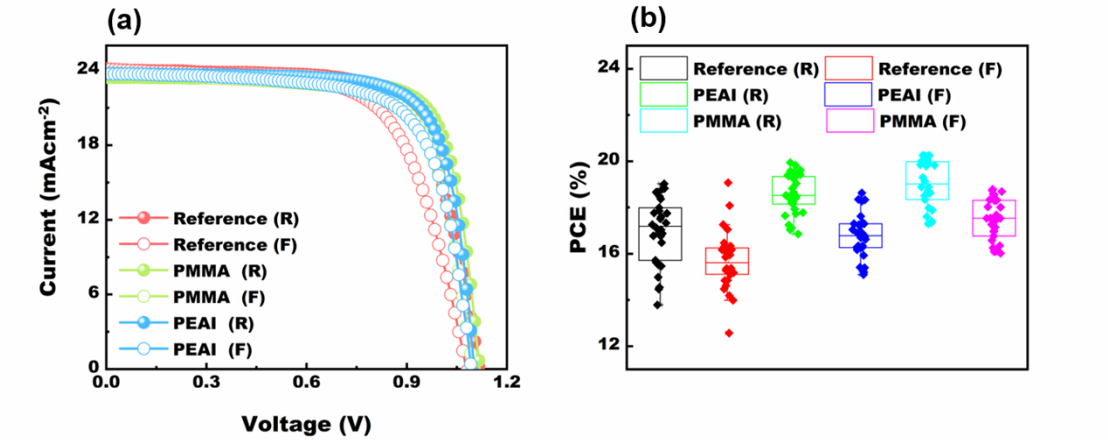

Figure S3. (a) J–V characteristics from forward scan (FS, J_{sc} to V_{oc}) and reverse scan (RS, V_{oc} to J_{sc}) determined under simulated AM 1.5G illumination for the reference, PEAI, PMMA devices. (b) box plots of FS-PCE and RS-PCE for the corresponding devices

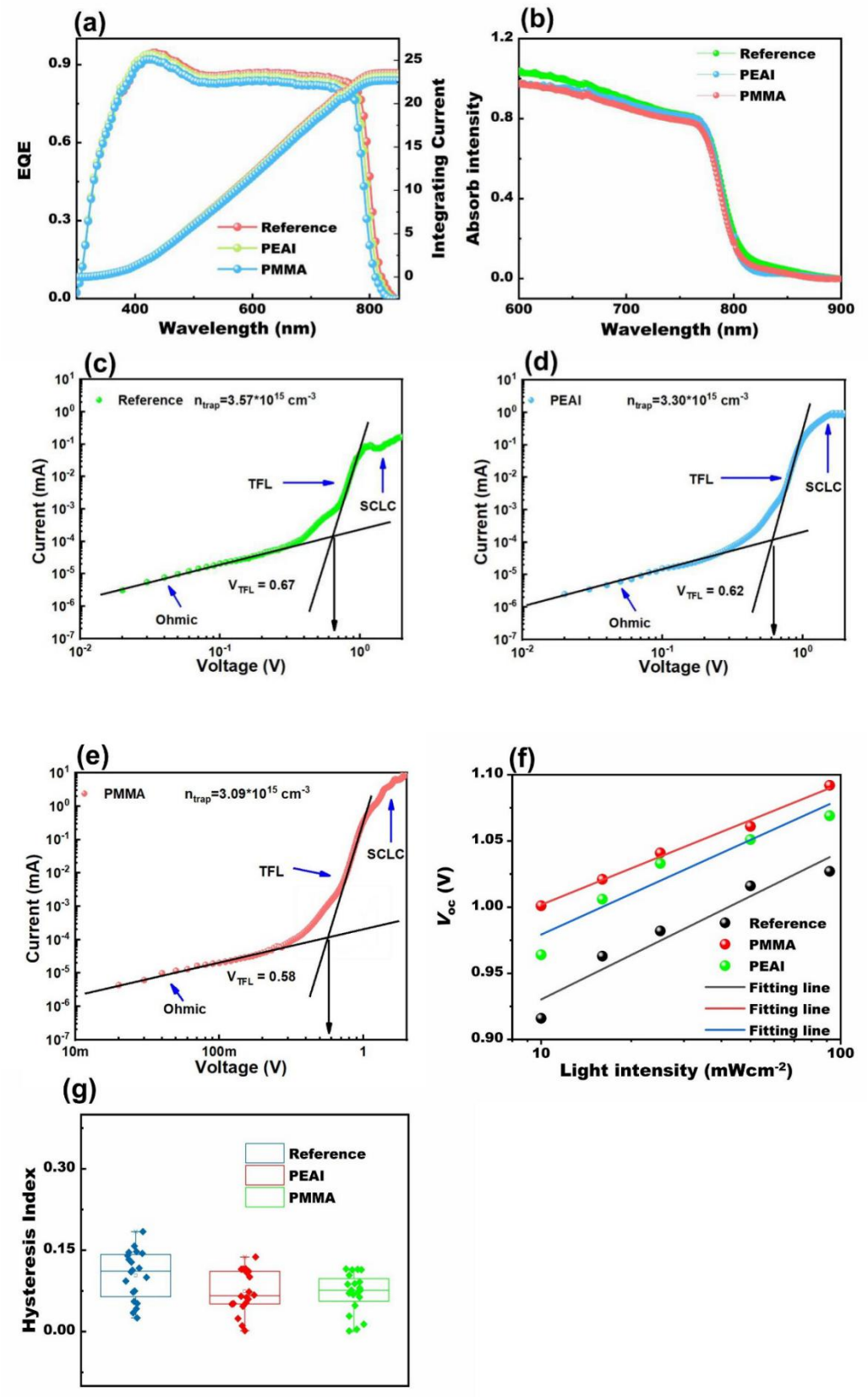

Figure S4. (a) EQE and corresponding integrated short current of the corresponding devices. (b) absorption spectrum of three type PSCs films in the visible region. (c, d and e) Dark current–

voltage curves of electron-only devices for reference (c), PEAI (d) and PMMA (e) device. (f) Relationship between V_{oc} and light intensity for different devices. (g)Box plots of hysteresis index for reference, PEAI and PMMA device.

2.2 Analysis of stability results

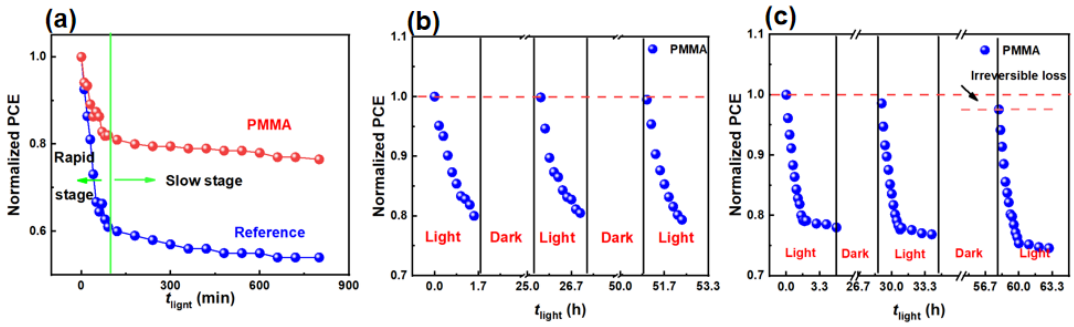

Figure S5. (a) The dependence of PCE on illumination time for the reference and PMMA device. The initial stage of rapid decay about $\leq$ 90 min is defined as the rapid stage and that about $\geq$ 90 min as the slow stage. (b) Reversible process: PMMA device is cyclically tracked 3 times for 90 min and it's left in dark at open circuit in between the consecutive measurements. (c) Irreversible process: PMMA device is cyclically tracked 3 times for 5 h and it's left in dark at open circuit in between the consecutive measurements.

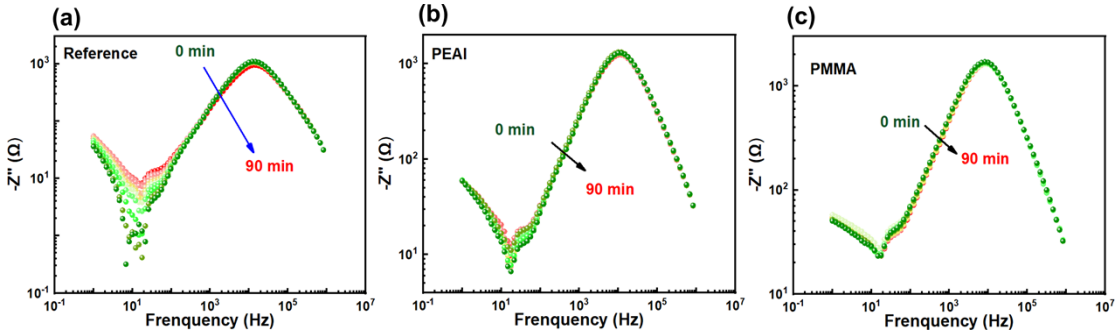

Figure S6. Relationship between negative imaginary component of impedance and frequency with the bias voltage time (a for reference, b for PEAI device and c for PMMA device)

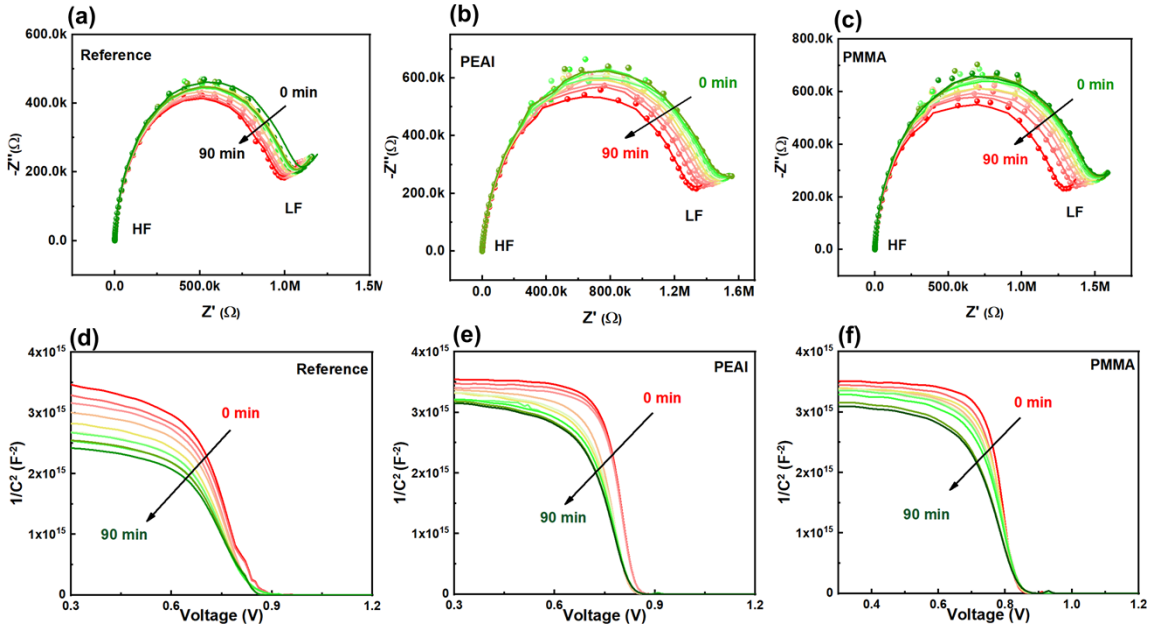

Figure S7. *Nyquist plots of three devices with the heat time (a for reference, b for PEAI and c for PMMA). Mott-Schottky plots carried out at 1 kHz for reference (d), PEAI device (e) and PMMA device (f).*

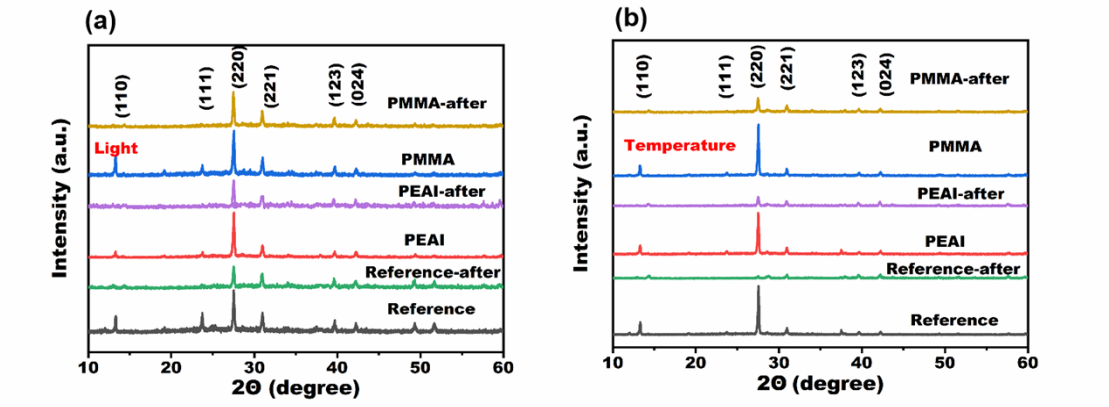

Figure S8. The X-ray diffraction tests on perovskite films before and after light or heat aging treatments for 90 min. The heating treatment results in more severely decreased (220) peaks.

Table.1 Performance parameters of three kinds of PSCs.

	J_{sc} (mAcm^{-2})	V_{oc} (V)	*FF*	PCE (%)
Reverse (reference)	24.056	1.117	70.056	18.828
Forward (reference)	24.142	1.078	65.458	17.048

Reverse (PEAI device)	23.747	1.102	75.694	19.818
Forward (PEAI device)	23.737	1.093	70.696	18.347
Reverse (PMMA device)	23.441	1.118	77.163	20.233
Forward (PMMA device)	23.759	1.097	71.297	18.591

Reference

1. Ravishankar S, Unold T, Kirchartz T. Comment on "Resolving spatial and energetic distributions of trap states in metal halide perovskite solar cells". Science, **2021**, 371, 6532.

2. Jiang Q, Zhao Y, Zhang X, et al. Nature Photonics, 2019, **13**, 460-466.

3. Chen Y, Meng Q, Xiao Y, et al. ACS applied materials & interfaces, 2019, **11**, 44101-44108.

4. K. Domanski, B. Roose, T. Matsui, M. Saliba, et.al. Energy. Environ. Sci., 2017, 10, 604-613.

5. H. Wang, A. Guerrero, A. Bou, A. M. Al-Mayouf and J. Bisquert, Energy. Environ. Sci., 2019, 12, 2054-2079.